IEEE Photonics Journal
An IEEE Photonics Society Publication

Open Access

Hybrid Switch of Correlation and Squeezing Using Resonant and Off-Resonant Excitation Spectrum in Nitrogen-Vacancy Center Diamond

Volume 11, Number 5, October 2019

Faizan Raza
Al Imran
Abubakkar Khan
Habib Ullah
Siqiang Zhang
Siqi Xiong
Irfan Ahmed
Yanpeng Zhang

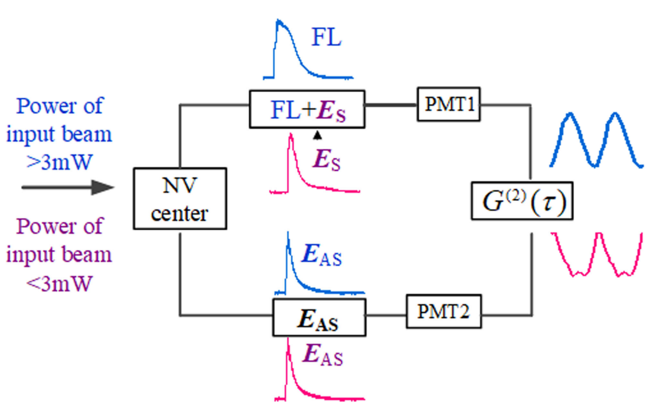

DOI: 10.1109/JPHOT.2019.2937790

Hybrid Switch of Correlation and Squeezing Using Resonant and Off-Resonant Excitation Spectrum in Nitrogen-Vacancy Center Diamond

Faizan Raza,[1] **Al Imran**,[1] **Abubakkar Khan**,[1] **Habib Ullah**,[1] **Siqiang Zhang**,[1] **Siqi Xiong**,[1] **Irfan Ahmed**,[2] **and Yanpeng Zhang**[1]

[1]Key Laboratory for Physical Electronics and Devices of the Ministry of Education & Shaanxi Key Laboratory of Information Photonic Technique, Xi'an Jiaotong University, Xi'an 710049, China
[2]Department of Physics, City University of Hong Kong, Hong Kong SAR

DOI:10.1109/JPHOT.2019.2937790

Manuscript received May 29, 2019; revised August 14, 2019; accepted August 22, 2019. Date of publication August 27, 2019; date of current version September 10, 2019. This work was supported in part by the National Key R&D Program of China under Grant 2017YFA0303700 and Grant 2018YFA0307500 and in part by the National Natural Science Foundation of China under Grant 61975159, Grant 61605154, Grant 11604256, Grant 11804267 and Grant 11904279. Corresponding author: Yanpeng Zhang (e-mail: ypzhang@mail.xjtu.edu.cn).

Abstract: Optical hybrid communication is one of the key fields of quantum communications, where scientists are focusing to integrate classical and quantum system as single hybrid system. In this regard, we realized optical hybrid switch using second-order fluorescence (FL) and spontaneous parametric four-wave mixing (SPFWM). The hybrid signal contains Stokes and the FL signal which can be distinguished using power of incident beam. In addition, we investigate the resonant and off-resonant excitation spectrum of negatively charged Nitrogen-vacancy (NV^-) center in diamond. The hybrid switch is realized by results obtained in time domain and intensity noise correlation. The optical hybrid switch can be controlled by power of incident beams. The hybrid index and temporal width contrast of the hybrid switch are about 4 and 90%, respectively.

Index Terms: (190.4380) nonlinear optics, four-wave mixing, (260.2510) fluorescence.

1. Introduction

Physicists have made credible progress in understanding and manipulating the electronic properties of single impurities. Since its first observation in late 1990s, the nitrogen-vacancy defect in diamonds has attracted a lot of interest in theoretical and experimental quantum physics [1]. The nitrogen-vacancy center exhibits quantum behavior that can be accessed with comparably simple experimental setup at room temperature. The negatively charged nitrogen-vacancy (NV^-) center in diamond is an individually addressable electronic spin that can be initialized and read out optically at room temperature [1]. Due to its high signal to background ratio, NV^- center makes sure that even a single bit of information is stored in a single photon [2]. The diamond NV^- center also has electron spin coherence time in milliseconds [3] credited to low phonon density of states and stability of the host material [4] inspired an exciting range of promising applications in solid state quantum computation [5]. Optical properties of diamond are of great interest because of the proposed application of diamond as a laser source and high efficiency photodetector for the UV [6]. Optical response detected using magnetic resonance experiments illustrated that the ground and excited states are spin triplets and the transition is labelled as ^{3}A-^{3}E [7]. Recent transient hole-burning research [7] exhibit that the fine structure splitting in excited state is mainly influenced by spin-spin interactions. A novel entanglement between two different types of states has been illustrated using the classical state and the quantum mechanical state for reliable quantum information processing using the hybrid state as a new kind of qubit [8]. This approach has gained significant appreciation due to its incorporation of the benefits of both non-classical and classical photon states, particularly for near-deterministic quantum teleportation using linear optics and hybrid qubits [9] and information transfer between different types of qubits [10]. The principal motivation of this work is to control hybrid state by using wavelength of the external laser in a diamond NV$^-$ center. Such results can find possible applications in long-distance communication and optical information storage.

We study an optical hybrid switch by spontaneous parametric four-wave mixing (SPFWM) and fluorescence (FL) using resonant and off-resonant excitation in diamond NV$^-$ center. The Stokes emission ($\boldsymbol{E_S}$) and fluorescence constitute the hybrid signal, whose propagation can be described as evolution under the Heisenberg picture. We investigated effect of power and wavelength of excitation laser on hybrid signal in both time and spectral domain. Also, we study two-mode intensity-noise correlation and intensity-difference squeezing between anti-Stokes and hybrid signals. We observed that the Stokes interacts with the FL and that the amplitude of correlation and squeezing can be switched by controlling the FL emission in hybrid signal. Moreover, an optical hybrid switch model was developed based on the competition between FL and Stokes in hybrid signal. Further, hybrid index and temporal width contrast of hybrid switch can be optimized by controlling power of incident beam.

2. Experimental Setup and Theory

The sample used in our experiment is a $<$100$>$ oriented crystal diamond and contains less than 5 ppb nitrogen concentration and typically has less than 0.03 ppb NV$^-$ center concentration. The sample was held in a cryostat which was maintained at 77 K by flowing liquid nitrogen. Figure 1(a) shows the schematic diagram of the experimental setup. Two dye lasers (narrow scan with a 0.04 cm^{-1} linewidth) pumped by an injection locked single-mode Nd:YAG laser (Continuum Powerlite DLS 9010, 10 Hz repetition rate, 5ns pulse width) were used to generate the two pumping fields $\boldsymbol{E_1}$ (frequency ω_1, wavevector $\boldsymbol{k_1}$, Rabi frequency G$_1$, wavelength 575 nm, coupling transition $|0\rangle \rightarrow |1\rangle$ with detuning $\Delta_i = \omega_{mn} - \omega_i$) and $\boldsymbol{E_2}$ (frequency ω_2, wavevector $\boldsymbol{k_2}$, Rabi frequency G$_2$, wavelength 637 nm, coupling transition $|0\rangle \rightarrow |2\rangle$). The pumping field $\boldsymbol{E}$i (where i = 1, 2) excites the sample and is reflected back from the surface of NV$^-$ in its original path, which is named as $\boldsymbol{E}$i$'$ with a small angle θ between them. Stokes ($\boldsymbol{E_S}$) and anti-Stokes ($\boldsymbol{E_{AS}}$) signals are generated via SPFWM process, satisfying the phase-matching condition $\boldsymbol{k_1} + \boldsymbol{k_1'} = \boldsymbol{k_S} + \boldsymbol{k_{AS}}$. Arrangements of three photomultiplier tubes (PMT 1–3) are used to detect the generated $\boldsymbol{E_S}$, $\boldsymbol{E_{AS}}$ and hybrid signals (FL + $\boldsymbol{E_S}$). Figure 1(b) shows the energy level scheme of the NV$^-$ center in diamond. The NV$^-$ center has two triplet states; named the ground state ^{3}A$_2$ and the excited state ^{3}E, and two singlet states (^{1}A$_1$, ^{1}E). The two triplet states ^{3}A$_2$ and ^{3}E are split into $|m_s = 0\rangle$ and $|m_s = \pm 1\rangle$ fine-structure levels as shown in Fig. 1(c). The energy difference between $|m_s = 0\rangle$ and $|m_s = \pm 1\rangle$ for ^{3}A$_2$ is D = 2.8 GHz while for excited state ^{3}E is D = 1.42 GHz [12]. Two level system ($|0\rangle \rightarrow |1\rangle$ and $|0\rangle \rightarrow |2\rangle$) is constructed using these fine-structure levels of NV$^-$ center.

In a two-level system, by opening field $\boldsymbol{E_1}$ the Stokes $\boldsymbol{E_S}$ and anti-Stokes $\boldsymbol{E_{AS}}$ signals are generated with phase-matching condition $\boldsymbol{k_S} = \boldsymbol{k_1} + \boldsymbol{k_1'} - \boldsymbol{k_{AS}}$ and $\boldsymbol{k_{AS}} = \boldsymbol{k_1} + \boldsymbol{k_1'} - \boldsymbol{k_S}$, respectively. The perturbation chains for the $\boldsymbol{E_S}$ and $\boldsymbol{E_{AS}}$ signals in the two-level system is written as $\rho_{10}^{(0)} \xrightarrow{E_1'} \rho_{10}^{(1)} \xrightarrow{E_{AS}} \rho_{00}^{(2)} \xrightarrow{E_1} \rho_{10(S)}^{(3)}$ and $\rho_{10}^{(0)} \xrightarrow{E_1} \rho_{10}^{(1)} \xrightarrow{E_S} \rho_{00}^{(2)} \xrightarrow{E_1'} \rho_{10(AS)}^{(3)}$, respectively. The third order

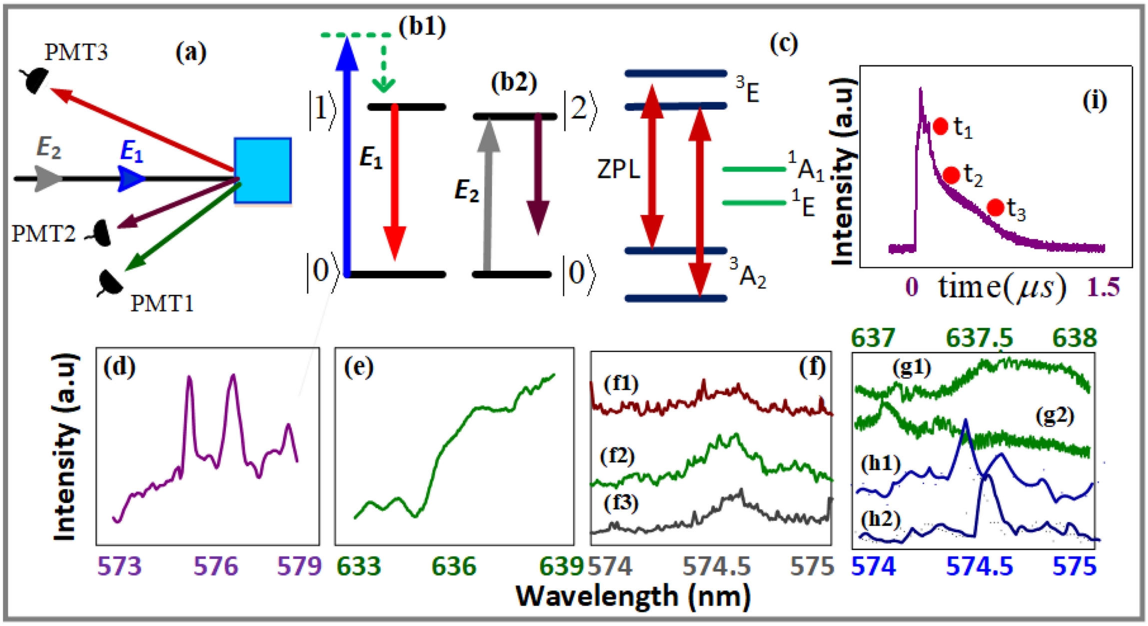

Fig. 1. (a) Experimental setup. (b1) and (b2) Two-level atomic system of NV$^-$ center excited by $\boldsymbol{E_1}$ (575 nm) and $\boldsymbol{E_2}$ (637 nm) input beam, respectively. (c) Energy level scheme of the NV$^-$ center. (d) and (e) Spectral intensity signal obtained by scanning $\boldsymbol{E_1}$ and $\boldsymbol{E_2}$ respectively, in a two-level system. (d) and (e) Spectral intensity signal obtained by scanning off-resonant $\boldsymbol{E_1}$ and resonant field $\boldsymbol{E_2}$, respectively. (f1)–(f3) spectral intensity signal controlled by changing $\boldsymbol{E_1}$ power (mW). (g1)–(g2) and (h1)–(h2) Spectral intensity signal measured at different gate positions (t_1 and t_2) by scanning $\boldsymbol{E_1}$ and $\boldsymbol{E_2}$, respectively. (i) Time domain signal from the NV$^-$ center, where t_1 (200 ns), t_2 (500 ns) and t_3 (900 ns) are different positions of boxcar gate.

nonlinear density matrix elements of the $\boldsymbol{E_S}$ and $\boldsymbol{E_{AS}}$ signals are given as [13], [14]

$$\rho_{10}^{(3)} = \frac{-iG_1G_1'G_{AS}}{(\Gamma_{10}+i\Delta_1)[\Gamma_{00}+i(\Delta_1'-\Delta_{AS})][\Gamma_{10}+i(\Delta_1+\Delta_{AS})]} \tag{1a}$$

$$\rho_{10}^{(3)} = \frac{-iG_1G_1'G_S}{(\Gamma_{10}+i\Delta_1)[\Gamma_{10}+i(\Delta_1-\Delta_S)(\Gamma_{00}+i(\Delta_1'-\Delta_S)]} \tag{1b}$$

Where $G_i = \mu_i E_i/\hbar$ is Rabi frequency of field $\boldsymbol{E_1}$, with the electric dipole matrix elements μ_{ij} of levels $|i\rangle$ and $|j\rangle$ and Γ_{ij} is the transverse decay rate. The decoherence rate of $\boldsymbol{E_S}/\boldsymbol{E_{AS}}$ is given as $\Gamma_{S/AS} = 2\Gamma_{10}+\Gamma_{00}$. In two-level system, with a strong pumping field switched on, the second-order fluorescence signal is generated through the perturbation chain $\rho_{00}^{(0)} \xrightarrow{E_1} \rho_{10}^{(1)} \xrightarrow{E_1'} \rho_{11}^{(2)}$, the diagonal density matrix element is given by $\rho_{11}^{(2)} = -|G_1|^2/(\Gamma_{10}+i\Delta_1+|G_1|^2/\Gamma_{00})\Gamma_{11}$. The decoherence rate of FL is given as $\Gamma_{FL} = \Gamma_{10}+\Gamma_{11}$.

In this experiment, coherent signals (Stokes/anti-Stokes) were generated from the SPFWM process, and non-coherent (hybrid) signals were obtained from cross-Kerr nonlinear processes. The SPFWM process produces Stokes and anti-Stokes signals. The cross-Kerr nonlinear processes produce hybrid (FL + $\boldsymbol{E_S}$) signal via the interaction of the FL with the Stokes photons. To generate the hybrid signal, we used a scheme similar to the one explained in [15] where the cross-Kerr nonlinearity is responsible for the interaction of the SPFWM and FL signals in the nonlinear crystal. Cross-Kerr nonlinearity is essential for the generation of an entangled state. The Kerr nonlinearity is characterized by a refractive index of $n_0 + n^2|E|^2$, where n_0 is the weak-field linear refractive index term and $n^2 = 3\chi^{(3)}/2n_0$ is a nonlinear refractive index. Because of the coherence of the nonlinear medium, the interaction between the SPFWM and FL outputs results in a hybrid signal ($\boldsymbol{E_S}$ + FL).

The combination of a common energy level, a strong pumping field, a dressing field and propagation through a common medium creates such an interaction between the generated signals and the FL. This effect also allows one to create strongly correlated states. [16], [17] The temporal intensity of the hybrid (FL + $\boldsymbol{E}_{\mathbf{S}}$) and pure $\boldsymbol{E}_{\mathbf{AS}}$ signals is given by

$$I_1(t) = \rho_S^{(3)} e^{-G_i^2 t^2} \otimes e^{-\Gamma_S t} + \rho_{FL}^{(2)} e^{(t-t_b)^2/w^2} \otimes e^{-\Gamma_{FL} t} \tag{2a}$$

$$I_2(t) = \rho_{AS}^{(3)} e^{-G_i^2 t^2} \otimes e^{-\Gamma_{AS} t} \tag{2b}$$

Where $G_i = -\mu E_i/\hbar$ is the Rabi frequency of the pumping fields, w is the pulse width, t_b, is the delayed time , $\Gamma_{FL/S/AS}$ is the decoherence rate. $I_1(t)$ and $I_2(t)$ is the output intensity signals detected at PMT1 and PMT3 respectively. The obtained intensity can be fit by time-domain multi-peak signals as $I(t) = A\int_{-\infty}^{t} d\tau^* e^{-2(\tau - t_0/\omega)} e^{-\Gamma(t-\tau)}$.

3. Correlation and Squeezing

The two-mode intensity noise correlation function $G_{ij}^{(2)}(\tau)$ between intensity fluctuations of two optical beams ($i, j, i \neq j$) as a function of time delay τ is given by [18]

$$G_{ij}^{(2)}(\tau) = \frac{\langle \delta I_i(t)\delta I_j(t+\tau)\rangle}{\sqrt{\left\langle [\delta I_i(t)]^2\right\rangle \left\langle [\delta I_j(t+\tau)]^2\right\rangle}} \tag{3}$$

In two-mode, the line shape of the correlation function for pure SPFWM is determined by [19]

$$A_{S/AS} = R_1|A_1|^2 \Big[e^{-2\Gamma^{+}{}_{S/AS}|\tau|} + e^{-2\Gamma^{-}{}_{S/AS}|\tau|} - 2\cos(\Omega_e|\tau|) e^{(\Gamma^{+}{}_{S/AS} + \Gamma^{-}{}_{S/AS})^{|\tau|}} \Big] \tag{4}$$

Similarly, the degree of two-mode intensity difference squeezing is given by [20]

$$Sq^{(2)} = Log_{10} \frac{\langle \delta^2(\hat{I}_i - \hat{I}_j)\rangle}{\langle \delta^2(\hat{I}_i + \hat{I}_j)\rangle} \tag{5}$$

Where $\langle \delta^2(\hat{I}_i - \hat{I}_j)\rangle$ is the mean square deviation of the intensity difference and $\langle \delta^2(\hat{I}_i + \hat{I}_j)\rangle$ is the mean square deviation of the intensity sum.

4. Results and Discussion

First, by scanning the pumping field $\boldsymbol{E}_1$ only, one can easily observe the off-resonant excitation spectrum of NV$^-$ center by collecting the emitted light. Figure 1(d) shows the hybrid signal from energy levels $|0\rangle$ and $|1\rangle$ in frequency domain by scanning $\boldsymbol{E}_1$ from 574 nm to 579 nm. The excitation spectrum signals were detected by fast gated PMT when scanning the laser frequency. The spectrum obtained at low temperature (77 K) exhibits a sharp peak located at about 574.5 nm and a slightly broad peak at about 576.7 nm shown in Fig. 1(d). The linewidth of two spectral peaks are determined by decay rate Γ_{10} and is measured between 0.1–0.5 nm. The two peaks observed in off-resonant excitation spectrum can be explained from fine structure energy level splitting from spin-spin interaction and induced crystal field effect of NV$^-$ center coupled with high photon induced mixing caused by off-resonant excitation. Figure 1(e) shows the resonant excitation spectrum by scanning $\boldsymbol{E}_2$ from 633 nm to 639 nm in a two-level system. In case of resonant excitation spectrum, no spectral peak is observed which can be explained from low photon inducing, weak spin-spin interaction and low crystal field effect at resonant excitation. In Fig. 1(f), we investigated optical behavior of off-resonant excitation (first peak shown in Fig. 1(d)) by changing power of $\boldsymbol{E}_1$ from 2 mW (Fig. 1(f1)) to 5 mW (Fig. 1(f3)). When power of $\boldsymbol{E}_1$ is at 5 mW, amplitude of spectral peak is very low due to low population transfer between ground and excited state as shown in Fig. 1(f1).

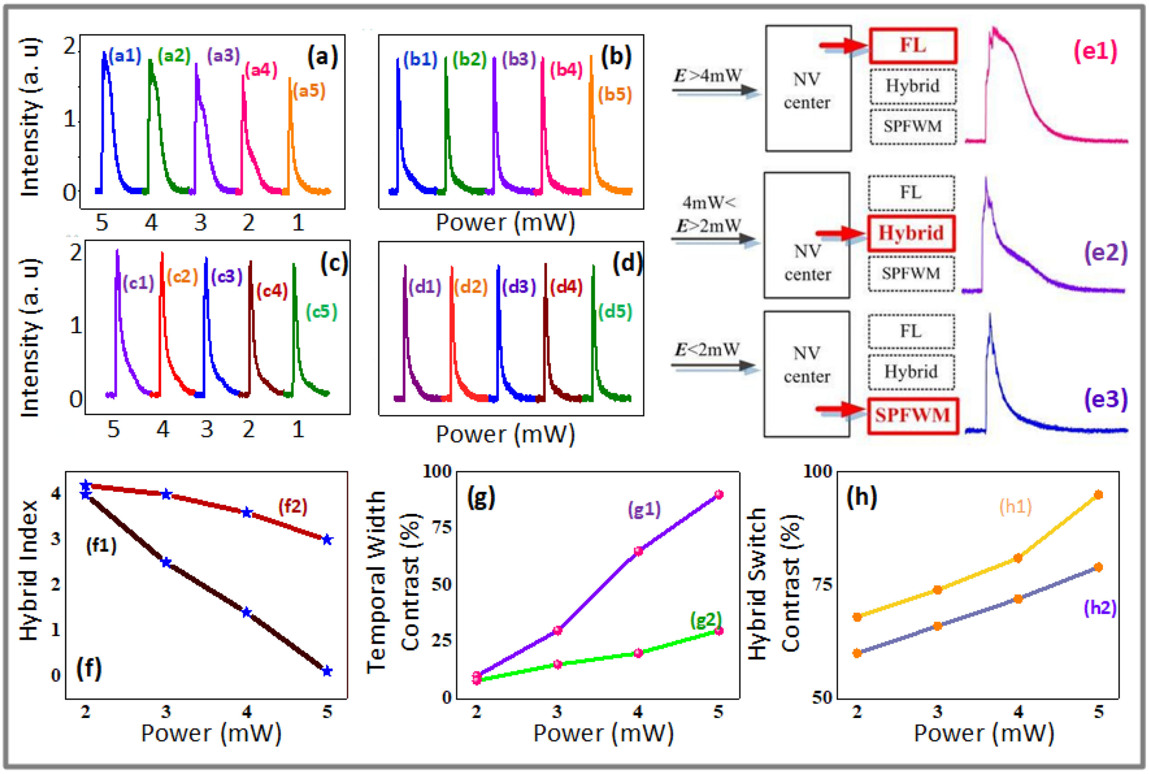

Fig. 2. The evolution of temporal intensity signal obtained from NV$^-$ center in two-level atomic system. (a1)–(a5) and (b1)–(b5) Intensity of the hybrid (FL + $\boldsymbol{E}_\mathbf{S}$) and pure $\boldsymbol{E}_\mathbf{AS}$ signal, respectively, when power of off-resonant beam $\boldsymbol{E}_\mathbf{1}$ is decreased from 5 mW to 2 mW. (c1)–(c5) and (d1)–(d5) Intensity of the hybrid (FL + $\boldsymbol{E}_\mathbf{S}$) and pure $\boldsymbol{E}_\mathbf{AS}$ signal in time domain as power of resonant beam $\boldsymbol{E}_\mathbf{2}$ (637 nm) decreases, respectively. (e) Proposed model of hybrid switch controlled by power of input beam $\boldsymbol{E}_\mathbf{1}$ power. (f1) and (f2) show trend of hybrid index when power of $\boldsymbol{E}_\mathbf{1}$ and $\boldsymbol{E}_\mathbf{2}$ is changed from low (2 mW) to high (5 mW), respectively. (g1) and (g2) show trend of temporal width contrast when power of $\boldsymbol{E}_\mathbf{1}$ and $\boldsymbol{E}_\mathbf{2}$ is changed from low (2 mW) to high (5 mW), respectively. (h1) and (h2) show trend of hybrid switch contrast when power of $\boldsymbol{E}_\mathbf{1}$ and $\boldsymbol{E}_\mathbf{2}$ is changed from low (2 mW) to high (5 mW), respectively.

With increase in power, amplitude of peak increases as shown in Fig. 1(f3), which can be explained from high photon induced mixing due to laser heating. Figures 1(g) and 1(h) shows dependence of resonant and off-resonant excitation spectrum on boxcar gate position (Fig 1(i)), respectively. Excitation spectrums in Figs. 1(g1) and 1(h1) are observed at gate position t_1 whereas excitation spectrum in Figs. 1(g2) and 1(h2) are observed at gate position t_3. In Figs. 1(g1–g2), resonant excitation spectrum does not show any variation with respect to change in gate position, which can be explained by weak effect of spin-spin interaction, crystal field effect and low photon inducing at resonant excitation. In off-resonant excitation spectrum peak becomes more prominent at gate position t_3 as shown in Fig. 1(h2).

Figure 2 represents the temporal intensities of the output hybrid and anti-Stokes signals in two level system. There are two peaks (sharp peak and broad peak) associated with hybrid signal in time domain emerging sequentially as shown in Fig. 2(e2). A sharp peak is followed by a broad peak. The Stokes signal (sharp peak) comes from the direct transition between states $|^3A_2, m_s = 0\rangle$ and $|^3E, m_s = 0\rangle$. The FL emission (broad peak) results from photon induced transitions from the $|^3E, m_s = \pm 1\rangle$ to $|^3A_2, m_s = \pm 1\rangle$. Since the generation of FL and $\boldsymbol{E}_\mathbf{S}$ emission is simultaneous, one can treat the recorded signal at PMT as hybrid signal. In two level system, a hybrid signal ($\rho_{11}^{(2)} + \rho_S^{(3)}$) that includes the $\boldsymbol{E}_\mathbf{S}$ produced by $\boldsymbol{E}_\mathbf{1}$ and $\boldsymbol{E}'_\mathbf{1}$ ($\boldsymbol{k}_\mathbf{S} = \boldsymbol{k}_\mathbf{1} + \boldsymbol{k}'_\mathbf{1} - \boldsymbol{k}_\mathbf{AS}$) along with FL is detected at PMT1. At PMT3, pure anti-Stokes signal $\boldsymbol{E}_\mathbf{AS}$ with phase matching condition $\boldsymbol{k}_{AS} = \boldsymbol{k}_1 + \boldsymbol{k}'_1 - \boldsymbol{k}_S$ is detected. Temporal intensity of hybrid ($I_1(t)$) and anti-Stokes ($I_2(t)$) signals is modeled by Eq. 2(a) and Eq. 2(b), respectively. The intensity of $\boldsymbol{E}_{\mathbf{S}}$ and FL signal are related to density matrix elements from Eq. (1) as $I_S \propto |\rho_S^{(3)}|^2$and $I_{FL} \propto |\rho_{11}^{(2)}|^2$ respectively. Figure 2(a) shows the time domain intensity of hybrid signal detected at PMT1 as the power of off-resonant beam $\boldsymbol{E}_{\mathbf{1}}$ ($\Delta_1 = 575.4$ nm) decreases from 5 mW (Fig. 2(a1)) to 2 mW (Fig. 2(a5)). Figure 2(b) shows time domain intensity of pure $\boldsymbol{E}_{\mathbf{AS}}$ signal (detected at PMT3) obtained under same conditions as in Fig. 2(a). Figure 2 shows increase in proportion of Stokes emission in hybrid signal as power of input beam decreases from 5 mW to 2 mW. When NV^- center is excited by $\boldsymbol{E}_{\mathbf{1}}$, most of particles are excited to $|^3E, m_s = \pm 1\rangle$ because of photon induced effect. Due to excitation of $\boldsymbol{E}_{\mathbf{1}}$ at high power, high photon induced mixing caused by strong laser heating results in the domination of particle transfer between $|^3E, m_s = \pm 1\rangle$. Hence, FL emission $\rho_{11}^{(2)}$ dominates Stokes emission$\rho_S^{(3)}$ in hybrid signal and pure broad peak is obtained as shown in Figs. 2(a1) and 2(e1). When the power of $\boldsymbol{E}_{\mathbf{1}}$ is reduced, the intensity $I_1(t)$ of the hybrid signal decreases, while the proportion of Stokes emission ($\rho_S^{(3)}$) increases. Emergence of pure sharp peak at low power in Fig. 2(a5) suggest the transition between $|m_s = 0\rangle$ is larger at low photon density. Figure 2(b) shows the temporal intensity of $\boldsymbol{E}_{\mathbf{AS}}$ signal recorded at PMT3 in two level system, with same experiment conditions as discussed for Fig. 2(a). The pure sharp peak is prominent at all powers of $\boldsymbol{E}_1$ due to position of detector. The PMT3 is placed far from the sample and can only detect SPFWM emission results from $|^3E, m_s = 0\rangle$. Figures 2(c) and 2(d) show the temporal intensity of hybrid signal for NV^- under the excitation of resonant beam $\boldsymbol{E}_2$. The $\boldsymbol{E}_2$ beam excites particles from the ground state $|^3A_2, m_s = 0\rangle$ to the excited state $|^3E, m_s = 0\rangle$. At low power (2 mW), the sharp peak is more prominent as coherent emission $\rho_{10(AS)}^{(3)}$ is strong as shown in Fig. 2(b5). When power of $\boldsymbol{E}_2$ is increased from low to high, intensity of $\boldsymbol{E}_{\mathbf{S}}$ ($I_S \propto |\rho_S^{(3)}|^2$) is slightly decreased (Fig. 2(b3)) as FL emission proportion in hybrid signal slightly increases due to photon induced mixing caused by laser heating and increase in gain effect at high power as shown Fig. 2(b1). Figure 2(d) show similar behavior of temporal intensity of anti-Stokes signal as discussed in Fig. 2(b).

The hybrid switch is realized by the time domain intensity results observed in Figs. 2(a–d). Hybrid Index ($H = I_S/I_{FL}$) is the ratio of amplitude of the Stokes emission (I_S) to the amplitude of FL (I_{FL}) in a hybrid signal. In our experiment, hybrid index H increases from 0.1 (Figs. 2(a1)) to 4 (Figs. 2(a5)) as power of input beam is decreased from 5 mW to 2 mW. These results can be explained from evolution of Stokes emission from FL in hybrid signal as power is decreased. The FL emission (broad peak) is dominant at high power which results in low hybrid index (Fig. 2(a1) and 2(e1)). Similarly, $\boldsymbol{E}_{\mathbf{S}}$ becomes prominent at low power of $\boldsymbol{E}_{\mathbf{1}}$ as shown in Fig. 2(a5) and 2(e3), hence hybrid index increases significantly. The increase in hybrid index indicates that hybrid signal which was behaving as FL signal at high power is switched to pure $\boldsymbol{E}_{\mathbf{S}}$ signal at low power. In case of $\boldsymbol{E}_2$ excitation, hybrid index increases from 3 (Fig. 2(c11)) to 4.2 (Fig. 2 (c5)) as power of input beam is decreased from 5 mW to 2 mW. By fixing $\boldsymbol{E}_2$ at high power, phonon induced dipole-allowed transitions from $|^3\mathrm{E}, \mathrm{m_s} = \pm 1\rangle$ along with fluorescence emission increases slightly but contribution of Stokes is still high in hybrid signal, hence, comparatively, high hybrid index (3) is observed. Figures 2(f1) and 2(f2) show behavior of hybrid index (corresponding to intensity curves shown in Figs. 2(a) and 2(c)) when power of off-resonant and resonant beam is changed from 2 mW to 5 mW, respectively. In comparison to resonant excitation, value of hybrid index measured under off-resonant excitation shows significant decrease with change in power, which can be explained from evolution of pure FL signal from pure $\boldsymbol{E}_{\mathbf{S}}$ in hybrid signal as power is increased as shown in Figs. 2(f1). In our experiment, we were unable to achieve perfect hybrid index i-e 1 ($I_S = I_{FL}$) due to following reasons. (I) The alignment of our experimental setup is not perfect. (II) The polarization of input dressing beam is not perfectly linearly polarized. From our experiment, temporal width contrast for intensity can be written as $C_t = \Delta t_{Hyb}/\Delta t_{\mathrm{S}}$, then $C_t = 90\%$ at high power (Fig. 2(a1) and 2(e1)) and $C_t = 10\%$ at low power (Fig. 2(a5) and 2(e3)) which can be associated with different lifetime and decay rate. Temporal width contrast observed for resonant excitation (maximum 30% as shown in Fig. 2 (c5)) is considerably low as compare to off-resonant excitation. Figures 2(g1) and 2(g2) show trend of temporal width contrast when power of off-resonant and resonant beam

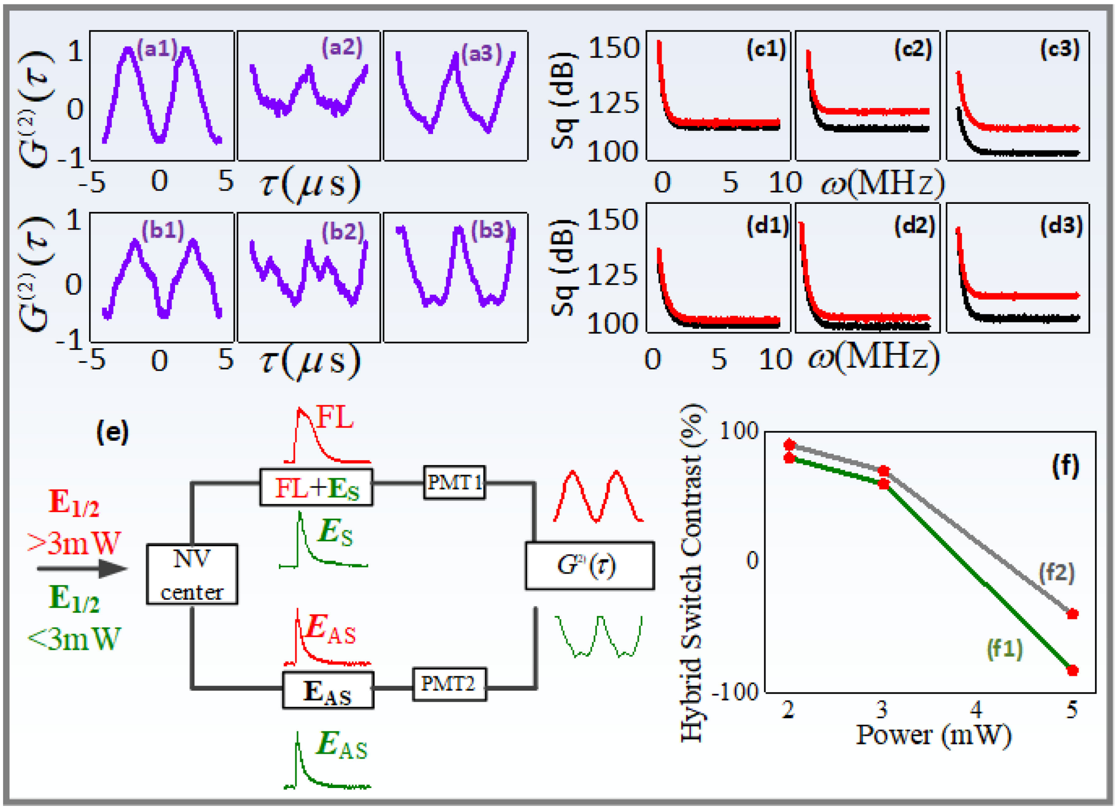

Fig. 3. (a1)–(a3) and (b1)–(b3) Two-mode intensity noise correlation between of hybrid signal (FL $+$ E_S) versus delayed time τ, controlled by changing power of $\boldsymbol{E_1}$ **and** E_2 from 5 mW to 2 mW, respectively. (c1)–(c3) and (d1)–(d3) shows the corresponding two-mode squeezing in accordance with (a1)–(a3) and (b1)–(b3), respectively. (e) Proposed model of hybrid switch in intensity noise correlation. (f1) and (f2) show trend of hybrid switch contrast when power of $\boldsymbol{E_1}$ and E_2 is changed from low (2 mW) to high (5 mW), respectively.

is changed from 2 mW to 5 mW, respectively. From Figs. 2(g1) and 2(g2), it can be concluded that value of temporal width contrast is high for $\boldsymbol{E_1}$ excitation, as FL emission with broad temporal width dominates at high power as compare to E_2 beam. The hybrid switch contrast is defined as $C_a = (A_{\max} - A_{\min})/(A_{\max} + A_{\min})$, the C_a is turn out to be 68% (Fig. 2(e3)) for Stokes emission at low power, whereas for FL emission $C_a = 95\%$ (Fig. 2(e1)) (where $A_{\max}$ and $A_{\min}$ are maximum and minimum intensities, respectively). Hybrid switch contrast for resonant excitation is measured as 59% (Fig. 2(c5)) and 79% (Fig. 2(c1)) at low and high power, respectively. Figures 2(h1) and 2(h2) show trend of hybrid switch contrast when power of off-resonant and resonant beam is changed from 2 mW to 5 mW, respectively. In Fig. 2(h), high value of hybrid switch contrast under off-resonant excitation can be explained from prominent switch from pure Stokes to pure fluorescence emission when power of off-resonant beam is increased from 2 mW to 5 mW. The switching speed of hybrid switch is about 18 ns and can be controlled by input field.

Herein, we investigated two-mode intensity noise correlation and squeezing of anti-Stokes and hybrid (FL $+$ E_S) signals by changing power of input beam from high (5 mW) to low (2 mW). For measuring two-mode correlation, we blocked the PMT2 and kept the rest of the PMTs on scanning mode. The time-dependent intensity fluctuations of the $\boldsymbol{E_{AS}}$ signal from PMT3 and hybrid signal from PMT1 are plotted using Eq. (3). The boxcar gated integrator were fixed at t_1. The total intensity of the hybrid signal is given by $\rho_{11}^{(2)} + \rho_S^{(3)}$. Figure 3(a) show two-mode intensity noise correlation of the anti-Stokes and hybrid signal as the power of off-resonant beam $\boldsymbol{E_1}$ decreases from 5 mW (Fig. 3(a1)) to 2 mW (Fig. 3(a3)). The competition between $\boldsymbol{E_S}$ and FL in hybrid signal determines

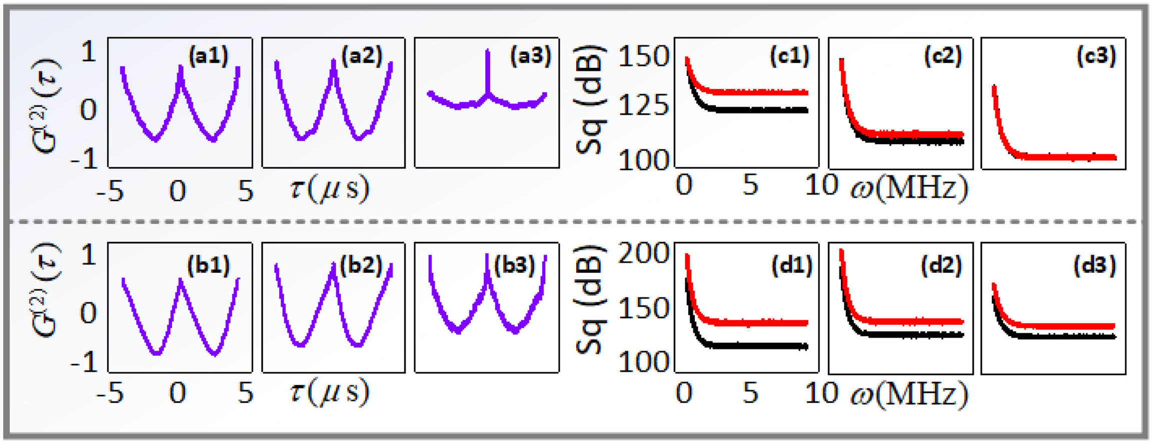

Fig. 4. (a1)–(a3) and (b1)–(b3) shows Two-mode intensity noise correlation of hybrid signal (FL + E_S) at different gate positions (t_1 (200 ns), t_2 (500 ns) and t_3 (900 ns)) when NV^- is excited by $\boldsymbol{E_1}$ and $\boldsymbol{E}_2$, respectively. (c1)–(c3) and (d1)–(d3) shows the corresponding two-mode squeezing in accordance with (a1)–(a3) and (b1)–(b3), respectively.

the sign of correlation function to be positive or negative. When the power of $\boldsymbol{E_1}$ is at 5 mW, intensity of FL emission $\rho_{11}^{(2)}$ dominates overall Stokes emission $\rho_S^{(3)}$ in hybrid signal due to high photon induced mixing which results in high particle transfer from the $|^3E, m_s = \pm 1\rangle$. At high power, hybrid signal behaves like pure FL signal and correlation function $G^{(2)}_{\mathrm{FL-AS}}(\tau)$ at delay time $\tau = 0$ has amplitude of -0.83 (Fig. 3(a1)), which can be explained by the no phase matching or energy conservation between the $\boldsymbol{E_{AS}}$ and the FL signal. When power $\boldsymbol{E_1}$ is gradually decreased, intensity of hybrid signal decreases whereas proportion of $\boldsymbol{E_S}$ emission increases (as discussed in Fig. 2) and hybrid signal acts as pure $\boldsymbol{E_S}$ signal as shown in Fig. 2(e3). At low power, the correlation peak $G^{(2)}_{S-AS}(\tau)$ at delay time $\tau = 0$ has amplitude of 0.83 shown in Fig. 3(a3). The $\boldsymbol{E_S}$ and $\boldsymbol{E_{AS}}$ photons are produced under the phase-matching and energy conservation condition. Hence, the $\boldsymbol{E_S}$ and $\boldsymbol{E_{AS}}$ signals are produced by each other, and the amplitude of correlation $G^{(2)}_{S-AS}(\tau)$ is high. Amplitude of correlation peak is switched from -0.83 (anti-correlated) to 0.83 (correlated) as power is decreased from 5 mW to 2 mW. Figure 3(b) show two-mode correlation of the $\boldsymbol{E_{AS}}$ and hybrid signal as the power of $\boldsymbol{E}_2$ (637nm) decreases from 5 mW (Fig. 3(b1)) to 2 mW (Fig. 3(b3)). When power of $\boldsymbol{E}_2$ decreases 5 mW to 2 mW, amplitude of correlation peak $G^{(2)}(\tau)$ is switched from -0.4 (Fig. 3(b1)) to 0.9 (Fig. 3(b3)). When power of resonant beam is kept at high, amplitude of correlation is high ($G^{(2)}(\tau) = -0.4$) as compare to off-resonant excitation ($G^{(2)}(\tau) = -0.83$) which suggest low FL emission under resonant excitation. Meanwhile, the two-mode intensity difference between the anti-Stokes and hybrid signals can be obtained by substituting the corresponding detected intensities into Eq. (5). From Eq. (5), we can also obtain the intensity difference $\delta^2(\hat{I}_i - \hat{I}_j)$ (red curve in Fig. 3(b1)) and the noise sum $\delta^2(\hat{I}_i + \hat{I}_j)$ (black curve in Fig. 3(b1)) versus ω (MHz). Similar to correlation, the value of intensity-difference squeezing shows a total increasing trend. The change of squeezing value with increase in power is shown in Figs. 3(c–d). The hybrid switch contrast of correlation is defined as $C_a = (A_{\max} - A_{\min})/(A_{\max} + A_{\min})$, then the value of C_a calculated at low and high power is 83% (Fig. 3(a3)) and -83% (Fig. 3(a1)), respectably. Where $A_{\max}$ and $A_{\min}$ are maximum and minimum amplitudes of correlation, respectively. For resonant excitation, hybrid switch contrast is calculated as 90% (Fig. 3(a3)) and -40% (Fig. 3(a1)) at low and high power, respectively. Comparatively. Hybrid switch contrast is high under $\boldsymbol{E}_2$ excitation due to strong SPFWM emission which results in high amplitude of correlation between $\boldsymbol{E_S}$ and $\boldsymbol{E_{AS}}$. Figures 3(f1) and 3(f2) show trend of hybrid switch contrast of correlation when power of $\boldsymbol{E_1}$ and $\boldsymbol{E}_2$ beam is changed from 2 mW to 5 mW, respectively.

Figures 4(a) and 4(b) show the two mode intensity noise correlation of hybrid signal and anti-Stokes under off-resonant and resonant excitation, respectively. The intensity fluctuations of hybrid and $\boldsymbol{E}_{\mathbf{AS}}$ signals are recorded by placing boxcar gate integrator at different positions as shown in Fig. 1(i). According to Eq. (4), line shape $A_{S/AS}$ of correlation signal is dependent on the decoherence rate. Figure 4(a) show correlation of the anti-Stokes and hybrid signal when gate position is changed from t_1 to t_3 (Fig. 1(i)) as the power of off-resonant beam $\boldsymbol{E}_{\mathbf{1}}$ is fixed at 3 mW. In the hybrid signal, since Stokes emission dominates at gate position at t_1 and FL signal with high decay rate $\Gamma_{FL} = \Gamma_{10} + \Gamma_{11}$ dominates at t_3, there is broad to sharp peak transition as gate position is changed from t_1 to t_3 as depicted in Fig. 4(a). Stokes signal with low decay rate $\Gamma_S = 2\Gamma_{10} + \Gamma_{00}$ is generated via coherent process whose linewidths are determined by atomic coherence time and are thus much narrower, which agrees with the transition of line shape from broad to sharp peak we observe in Fig. 4(a1) and (a3). Figure 4(b) show similar behavior of correlation line-shape for resonant excitation as discussed in Fig. 2(b). However, in Fig. 4(b3), sharp peak is less prominent at gate position t_3, which can be explained from low FL emission from $|^3E, m_s = \pm 1\rangle$ under resonant excitation. The value of intensity-difference squeezing shows a decreasing trend as gate position is changed, which is in accordance with our results discussed in Fig. 3. The change of squeezing value with change in gate position is shown in Figs. 4(c)–(d). From Fig. (4), one can see that, this experiment provides an accurate physical mechanism for hybrid switch due to the competition between FL and Stokes in a hybrid channel. The temporal width contrast for correlation is calculated from $C_\tau = \Delta\tau_{S-AS}/\Delta\tau_{hyb-AS}$, then $C_\tau = 90\%$ for $G^{(2)}_{S-AS}(\tau)$ (Fig. 4(a1)) is found to be 90% broader than $G^{(2)}_{FL-AS}(\tau)$ (Fig. 4(a3)), which can be explained from higher lifetime and faster decaying of SPFWM (lower Γ) corresponds to broad line shape of correlation function mentioned in Eq. 4.

5. Conclusion

In conclusion, we have presented a model of hybrid switch by using FL and SPFWM processes in NV^- center under phase matching conditions using resonant and off-resonant excitation. The hybrid signal was obtained by exciting NV^- center with off-resonant field. Also, resonant and off-resonant temporal and spectral signal dependence on spin-spin interaction and crystal field effect is discussed. Evolution of Stokes emission from FL in hybrid signal with decreasing power of input beam is also investigated. It is found out that the competition effect between SPFWM and FL signals determines the two-stage shape of intensity noise correlation and magnitude of squeezing. In addition, our results show that correlation change to anti-correlation when power of input beam decreases. By controlling power of input beams, hybrid switch contrast and switching speed of hybrid switch was optimized at 95% and 20 ns, respectively. We believed that our proposed system may have potential applications in optical hybrid communication.

References

[1] A. Gruber, A. Dräbenstedt, C. Tietz, L. Fleury, J. Wrachtrup, and C. V. Borczyskowski, "Scanning confocal optical microscopy and magnetic resonance on single defect centers," *Science*, vol. 276, no. 5321, pp. 2012–2014, 1997.

[2] M. V. G. Dutt *et al.*, "Quantum register based on individual electronic and nuclear spin qubits in diamond," *Science*, vol. 316, no. 5829, pp. 1312–1316, 2007.

[3] N. Bar-Gill, L. M. Pham, A. Jarmola, D. Budker, and R. L. Walsworth, "Solid-state electronic spin coherence time approaching one second," *Nat. Comm.*, vol. 4 p. 1743, 2013.

[4] C. Kurtsiefer, S. Mayer, P. Zarda, and H. Weinfurter, "Stable solid-state source of single photons," *Phys. Rev. Lett.*, vol. 85, no. 2, p. 290, 2000.

[5] F. Jelezko, T. Gaebel, I. Popa, M. Domhan, A. Gruber, and J. Wrachtrup, "Observation of coherent oscillation of a single nuclear spin and realization of a two-qubit conditional quantum gate," *Phys. Rev. Lett.*, vol. 93, no. 13, p. 130501, 2004.

[6] S. Koizumi, K. Watanabe, M. Hasegawa, and H. Kanda, "Ultraviolet emission from a diamond pn junction," *Science*, vol. 22, no. 5523, pp. 1899–1901, 2001.

[7] N. R. S. Reddy, N. B. Manson, and E. R. Krausz, "Two-laser spectral hole burning in a colour centre in diamond," *J. Lumin.*, vol. 38, no. 1–6, pp. 46–47, 1987.

[8] J. P. D. Martin, "Fine structure of excited 3E state in nitrogen-vacancy centre of diamond," *J. Lumin.*, vol. 81, no. 4, pp. 237–247, 1999.

[9] H. Jeong *et al.*, "Generation of hybrid entanglement of light," *Nat. Phot.*, vol. 8, no. 7, p. 564, 2014.

[10] S. W. Lee and H. Jeong, “Near-deterministic quantum teleportation and resource-efficient quantum computation using linear optics and hybrid qubits,” *Phys. Rev. A*, vol. 87, no. 2, p. 022326, 2013.
[11] K. Park, S. W. Lee, and H. Jeong, “Quantum teleportation between particle like and field like qubits using hybrid entanglement under decoherence effects,” *Phys. Rev. A*, vol. 86, no. 6, p. 062301, 2012.
[12] R. Schirhagl, K. Chang, M. Loretz, and C. L. Degen, “Nitrogen-vacancy centers in diamond: nanoscale sensors for physics and biology,” *Ann. Rev. Phys. Chem.*, vol. 65, pp. 83–105, 2014.
[13] Y. Zhang, A. W. Brown, and M. Xiao, “Opening four-wave mixing and six-wave mixing channels via dual electromagnetically induced transparency windows,” *Phys. Rev. Lett.*, vol. 99, no. 12, p. 123603, 2007.
[14] Y. Zhang, U. Khadka, B. Anderson, and M. Xiao, “Temporal and spatial interference between four-wave mixing and six-wave mixing channels,” *Phys. Rev. Lett.*, vol. 102, no. 1, p. 013601, 2009.
[15] C. C. Gerry, “Generation of optical macroscopic quantum superposition states via state reduction with a Mach-Zehnder interferometer containing a Kerr medium,” *Phys. Rev. A*, vol. 59, no. 5, p. 4095, 1999.
[16] M. O. Scully and M. Z. Suhail, “Quantum optics cambridge university press,” Cambridge CB2 2RU, 1997.
[17] S. A. Cummer and D. Schurig, “One path to acoustic cloaking,” *New J. Phys.*, vol. 9, no. 3, p. 45, 2007.
[18] M. D. Lukin, A. B. Matsko, M. Fleischhauer, and M. O. Scully, “Quantum noise and correlations in resonantly enhanced wave mixing based on atomic coherence,” *Phys. Rev. Lett.*, vol. 82, no. 9, p. 1847, 1999.
[19] H. X. Chen *et al.*, “Parametric amplification of dressed multi-wave mixing in an atomic ensemble,” *Las. Phy. Lett.*, vol. 11, no. 4, p. 045201, 2014.
[20] V. Boyer, A. M. Marino, R. C. Pooser, and P. D. Lett, “Entangled images from four-wave mixing,” *Science*, vol. 321, no. 5888, pp. 544–547, 2008.